

# Fast ion transport at solid-solid interfaces in hybrid battery anodes

Zhengyuan Tu<sup>1,5</sup>, Snehashis Choudhury<sup>2,5</sup>, Michael J. Zachman<sup>3</sup>, Shuya Wei<sup>2</sup>, Kaihang Zhang<sup>2</sup>, Lena F. Kourkoutis<sup>3,4</sup> and Lynden A. Archer<sup>1,2</sup>\*

Carefully designed solid-electrolyte interphases are required for stable, reversible and efficient electrochemical energy storage in batteries. We report that hybrid battery anodes created by depositing an electrochemically active metal (for example, Sn, In or Si) on a reactive alkali metal electrode by a facile ion-exchange chemistry lead to very high exchange currents and stable long-term performance of electrochemical cells based on Li and Na electrodes. By means of direct visualization and ex situ electrodeposition studies, Sn-Li anodes are shown to be stable at 3 mA cm<sup>-2</sup> and 3 mAh cm<sup>-2</sup>. Prototype full cells in which the hybrid anodes are paired with high-loading LiNi<sub>0.8</sub>Co<sub>0.15</sub>Al<sub>0.05</sub>O<sub>2</sub>(NCA) cathodes are also reported. As a second demonstration, we create and study Sn-Na hybrid anodes and show that they can be cycled stably for more than 1,700 hours with minimal voltage divergence. Charge storage at the hybrid anodes is reported to involve a combination of alloying and electrodeposition reactions.

echargeable batteries can efficiently store and convert chemical energy to electricity and thus are of increasing interest in a growing set of practices, including consumer electronics, advanced robotics, grid storage and electrified transportation<sup>1-4</sup>. To keep pace with constantly increasing performance demands, progress is required to design energy storage systems able to safely and reversibly store electrical energy with high energy density, high efficiency and long lifetime<sup>5-8</sup>. It has been commonly understood that the exploration of new electrochemically active materials that undergo efficient reduction/oxidation chemistry and possess considerably higher energy per unit mass/volume than those used in state-of-the-art batteries represents an important direction towards the energy storage breakthroughs sought in applications<sup>9-11</sup>.

The carbonaceous anode of a lithium ion battery (LIB) can be replaced by a metallic lithium anode with ten times the specific energy (3,860 mAh g<sup>-1</sup> versus 360 mAh g<sup>-1</sup>), which in principle should enable advanced high-energy non-lithiated cathodes such as sulfur or oxygen, so that the energy storage density of the whole cell can be significantly improved. Even more exciting cost and performance profiles are possible with room-temperature versions of these batteries that utilize metallic sodium or aluminium as the anode<sup>12,13</sup>. Challenges associated with developing reversible, safe and cost-effective high-energy rechargeable batteries based on any of these chemistries have become increasingly well known<sup>6,14</sup>. The most difficult issues stem from the fact that the highly electrochemically active materials at the anode are either naturally unstable against commonly used electrolytes or promote uncontrolled formation of rough, fragile solid-electrolyte interphases (SEIs). Although the concept of using spontaneously formed SEIs on the anode to regulate these events is not unfamiliar to the field, as it has long been known for lithiated graphite anodes in LIBs, information regarding their formation mechanism and detailed methods for controlling their structure/composition remain lacking<sup>15,16</sup>. The fact that the state-of-the-art LIBs render very high Coulombic efficiency and thus minimal energy loss during cycling underscores the criticalness of a well-defined, stable SEI<sup>17</sup>.

Unfortunately, these benefits are not easily realized in anodes based on energetic metals such as aluminium, lithium or sodium, as well as silicon and tin because their naturally grown SEIs are fragile, non-homogeneous (in terms of both morphology and composition), and the electrodes undergo substantial volume change during charge–discharge cycling. Thus, whether the charge-storage reaction relies on alloy formation, intercalation or plating of the active metal at the battery anode, the SEI formed naturally at any of these anodes undergoes repeated breakage and reformation processes during battery cycling, which is a parasitic cycle that consumes electrolyte and salt<sup>18</sup>. Moreover, if the electrode process requires metal plating, even at moderate current densities the conductivity inhomogeneity promotes selective electrodeposition on sparse local sites where mossy dendrites can proliferate.

A successful SEI for reactive metal anodes must have several properties including uniform contact with the electrode, high interfacial conductivity, and stable mechanical and electrochemical properties during battery cycling<sup>6,7</sup>. Previous studies have shown that crosslinked polymers<sup>19,20</sup>, ceramics<sup>21</sup> and composites<sup>22-25</sup> prevent dendrite proliferation by slowing deposition kinetics at rough regions on an electrode26. A number of works have also shown that single-ion conductors<sup>27–29</sup> and ionic liquids<sup>12,30</sup> limit concentration polarization above the diffusion-limited current, thereby suppressing electroconvective instabilities. Molecular species including vinylene carbonate, LiNO<sub>3</sub> and fluorinated ethylene carbonate<sup>31,32</sup> have also emerged as effective electrolyte additives for stabilizing metal electrodes. Artificial SEIs composed of polymers<sup>33,34</sup>, inorganic conductive compounds<sup>35,36</sup>, nanoparticles<sup>37,38</sup>, thin film<sup>39</sup>, carbon materials<sup>40,41</sup> and so on have likewise been reported to isolate the electrodes from parasitic side reactions with anions or solvent components in liquid electrolytes.

<sup>1</sup>Department of Materials Science and Engineering, Cornell University, Ithaca, NY, USA. <sup>2</sup>Robert Frederick Smith School of Chemical and Biomolecular Engineering, Cornell University, Ithaca, NY, USA. <sup>3</sup>School of Applied and Engineering Physics, Cornell University, Ithaca, NY, USA. <sup>4</sup>Kavli Institute at Cornell for Nanoscale Science, Cornell University, Ithaca, NY, USA. <sup>5</sup>These authors contributed equally: Zhengyuan Tu and Snehashis Choudhury. \*e-mail: laa25@cornell.edu

ARTICLES NATURE ENERGY

Here, we show that the formation of artificial interphases composed of an electrochemically active metal that stores charge by alloying reactions on an alkali metal anode leads to hybrid electrodes that utilize alloying and electrodeposition reactions to overcome the most serious challenges with sodium and lithium electrodes. Specifically, we take advantage of a facile ion-exchange chemistry performed in a carbonate electrolyte to rapidly deposit conformal coatings of tin onto sodium or lithium electrodes. By controlling the thickness of these coatings to nanometre dimensions, we further show that they perform multiple beneficial functions, including protecting the alkali metal electrode against parasitic reactions, providing a compliant interphase to accommodate volume changes associated with both the alloying and plating processes, and suppressing dendrite formation. In cells where the alloying and plating reactions occur at similar potentials, we find fast, unhindered ion transport across the solid-solid interface. By these means, we find that Sn-Li and Sn-Na anodes enable high-capacity, dendritefree battery cycling in both symmetric cells and in prototype cells in which Sn-Li is paired with LiNi<sub>0.8</sub>Co<sub>0.15</sub>Al<sub>0.05</sub>O<sub>2</sub>(NCA) electrodes with nominal specific capacity of 190 mAh g-1. The benefits of the approach are quite dramatic for sodium electrodes, which are notorious for their reactivity and propensity to form large, fragile dendritic deposits30 that easily break. It is observed that Sn-Na anodes cycle stably for > 1,000 hours in normally reactive electrolytes.

## Structural and transport characterization of Sn-Li anodes

The hybrid anodes used in the study were prepared by a simple surface ion-exchange reaction in a commonly used aprotic liquid lithium electrolyte, 1 M LiPF<sub>6</sub> in an ethylene carbonate-dimethyl carbonate (EC/DMC) solvent blend containing a second salt (see Fig. 1a)<sup>42</sup>. We focus on Sn because much is known about the electrochemical behaviour of the metal and its oxides<sup>43,44</sup>, including the fast interdiffusion of Li in Sn and the < 500 mV separation between Li–Sn alloy formation and Li plating. The treatment process is also fast and spontaneous due to the large electronegativity difference between alkali metals and metallic tin. Depending on the concentration of Sn salt employed, the appearance of the lithium surface after treatment ranges from dark brown to dark grey. The surface and the cross-sectional morphology of Sn–Li was interrogated without risk of contamination using a cryo-focused ion beam-scanning electron microscope (cryo-FIB-SEM). Figure 1b–e

shows images captured at  $-165\,^{\circ}\text{C}$  of Sn–Li using a  $10\,\text{mM}$  tin salt. It is evident that a tri-layer structure is formed. The top layer is the frozen electrolyte; the second is a tin-rich layer with thickness on the order of  $500\,\text{nm}$  composed of nanoparticles with average size around  $200\,\text{nm}$ . Energy-dispersive X-ray spectroscopy (EDX) mapping confirms that Sn is present in the nanoparticles, but no Sn is observed in the first layer. The bird's eye view of the Sn–Li anode deduced from room-temperature SEM reveals a uniform distribution of Sn nanoparticles on the surface of Li, a morphology quite distinctive from the pristine lithium.

To confirm the structure and chemistry of the Sn-Li hybrid electrode, X-ray diffraction (XRD) was employed (see Fig. 2a). The lithium metal used in the analysis was treated with electrolytes containing 1, 10 and 100 mM Sn salt. At the lowest concentration, only lithium metal signals and a minor lithium oxide peak at 32.6 degrees are observed. This indicates that the reaction is inhibited probably due to the low activity of Sn ions. Peaks at 31.1, 32.4, 44.1 and 45.2 degrees start to appear when the concentration is increased to 10 mM, suggesting that metallic tin with a structure following the R3m space group is formed. Increasing the salt concentration to 100 mM, the Sn layer alloys with Li as is evidenced by the peaks labelled with asterisks, which correspond to a Li<sub>5</sub>Sn<sub>2</sub> phase. The thickness of the Sn overlayer is estimated to be 2 µm with a compact, solid-like structure, as shown in Supplementary Figs. 2 and 3. The surface morphology is glassy with grain gaps among alloy terraces, possibly due to the formation of a Zintl phase that is naturally ionic and brittle<sup>45,46</sup>. Owing to their more uniform morphologies, electrochemical properties of Sn-Li anodes created using the 10 mM electrolyte (~500 nm coating thickness) are evaluated in detail. Compared to the thickness of the Li electrode (450 µm for bulk lithium or 45 µm for thin lithium studied later), the Sn coating thickness is low. As both the Sn and Li components are able to reversibly store Li by alloying and plating processes, respectively, lithium batteries that rely on mixed storage mechanisms are possible. The binary lithium plating/alloying energy storage modes on the interphase between the anode and the electrolyte are expected to work in synergy with the surface protection feature provided by the Sn SEI.

Knowledge of the charge transport processes at Sn-based electrode/electrolyte interphases can be deduced from impedance spectroscopy. Figure 2b compares the temperature-dependent Nyquist

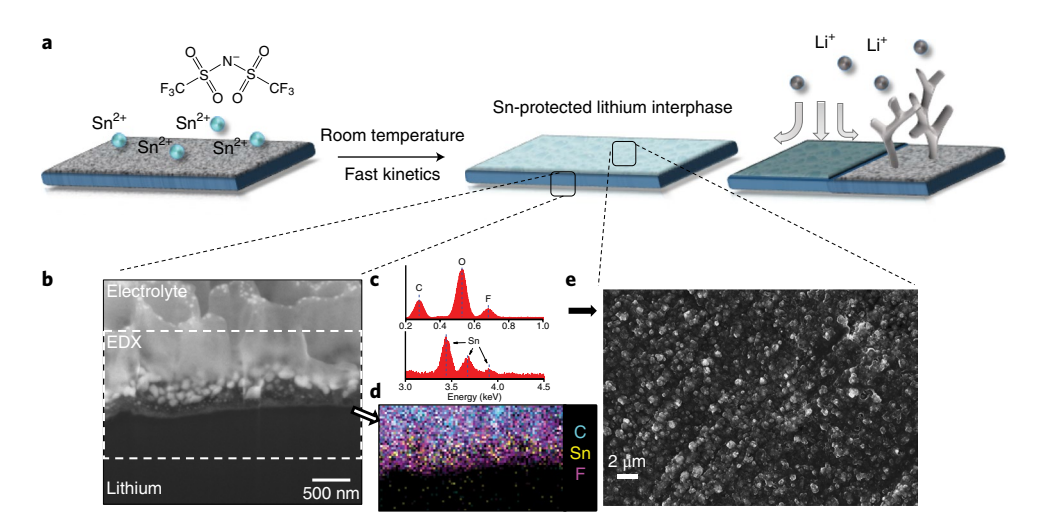
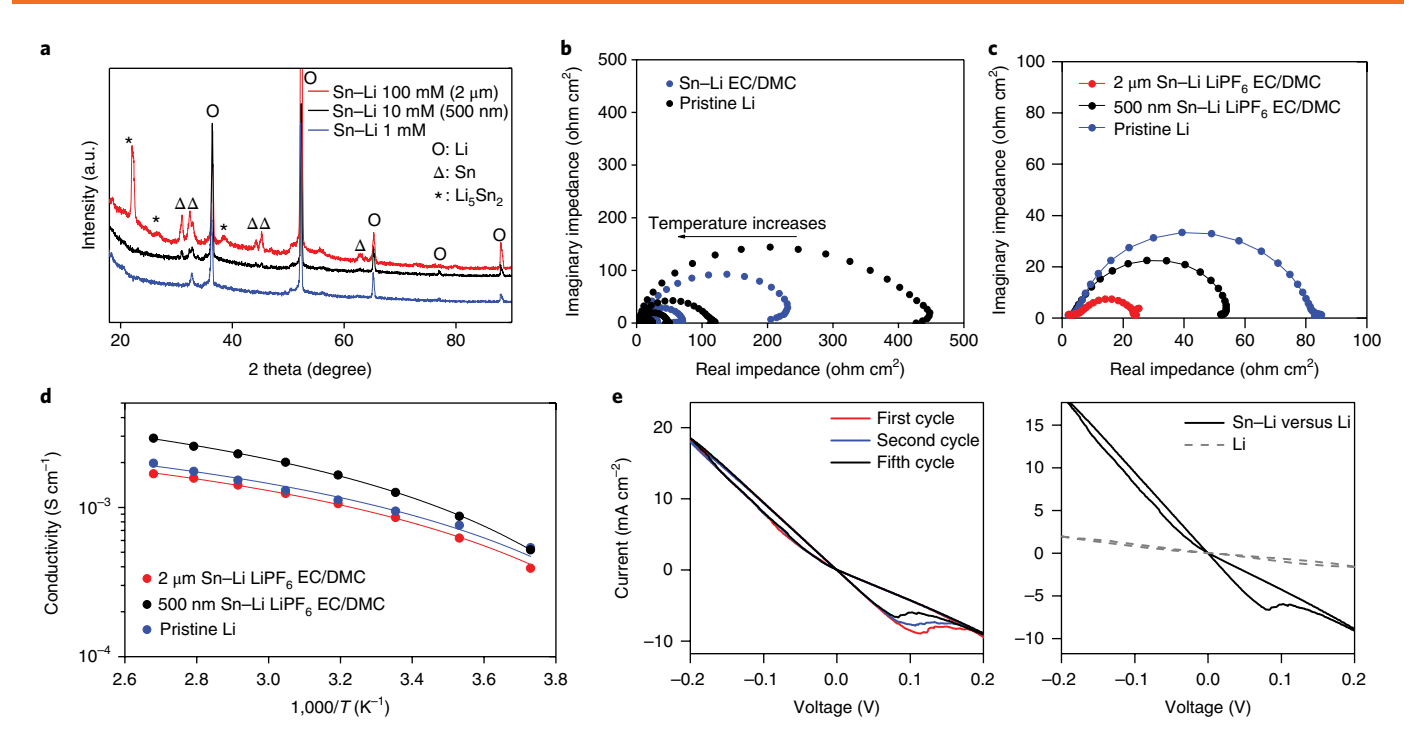


Fig. 1 | Hybrid anodes based on facile and fast Sn deposition on reactive metals produced by ion exchange. a, A schematic illustration of the tin protection on the lithium metal electrode. b, A cross-section cryo-FIB-SEM image of the tin-protected lithium, with dashed lines showing the EDX location. c, Typical EDX spectra of tin-protected lithium. d, EDX elemental mapping of fluorine (magenta) and tin (yellow) in the dashed rectangular region in Fig. 1b. e, Room-temperature field-emission SEM image of the surface morphology of the tin-protected lithium.

NATURE ENERGY ARTICLES



**Fig. 2 | Physical and electrochemical analysis of Sn-Li hybrid electrodes. a**, XRD profiles of tin-protected lithium prepared from the tin-bearing electrolyte with concentrations of 1 mM, 10 mM and 100 mM. **b**, Impedance spectra of symmetric lithium cells with tin-protected lithium and pristine lithium at a range of temperatures from –5 to 100 °C. **c**, A comparison of impedance spectra of symmetric lithium cells with tin-protected lithium and pristine lithium at room temperature. **d**, Temperature-dependent ionic conductivity of symmetric lithium cells with tin-protected lithium and pristine lithium. **e**, Left: cyclic voltammogram for cells with Sn-Li hybrid electrodes scanned at 1 mV s<sup>-1</sup>, for the first, second and fifth cycle. Right: comparison of cyclic voltammograms for symmetric cells containing Sn-Li hybrid and pristine Li electrodes scanned at a fixed rate of 1 mV s<sup>-1</sup>.

plots of symmetric Sn-Li electrodes and pristine lithium in a EC/ DMC electrolyte. Each spectrum can be fitted into the equivalent circuit model to decouple the interfacial transport resistance from other processes. As expected, the interfacial resistance decreases with increasing temperature (see Supplementary Fig. 4). The data are well described by a quasi-Arrhenius form in the intermediate temperature region, implying that the interfacial transport is thermally activated. Only one semicircle appears in the spectra, which indicates that the tin protection introduces no additional interfacial transport resistance. In fact, the interfacial resistance of cells using Sn-Li anodes is gradually lowered with increasing concentration of tin-bearing electrolyte (see Fig. 2c). A nearly threefold decrease (from approximately 80 Ohm cm<sup>2</sup> (pristine) to 25 Ohm cm<sup>2</sup> (2 µm tin protection)) of the interfacial resistance is observed. This result demonstrates that ion transport through the Sn SEI is unhindered and perhaps even promoted, which we suspect comes from fast charge transfer kinetics at the Sn-Li interface. It is well known that because of its reactivity with oxygen, Li foil forms an insulating oxide layer on its surface even when stored in an argon-filled glovebox. By treating the lithium with tin-bearing electrolyte, the oxidized layer is replaced by electrochemically active Sn nanostructures, which significantly facilitate ion transport through the SEI. Evidence in support of this point is presented in Supplementary Fig. 5, where the interfacial impedance of Sn-Li exposed to air is reported as a function of time. It is clearly seen that the Sn overlayer leads to enhanced chemical stability of the interface, which would enable integration of such electrodes in conventional dryroom manufacturing processes. The temperature-dependent ionic conductivity of electrolytes in contact with the Sn-Li anodes is reported in Fig. 2d for various Sn coating thicknesses. The conductivity exhibits a Vogel-Fulcher-Tamman temperature dependence in all cases, and cells based on the 500 nm Sn layer exhibit the highest ionic conductivity  $(1.3\,\mathrm{mS\,cm^{-1}}$  at  $25\,^{\circ}\mathrm{C})$ . Considering that essentially the same electrolyte is used in the measurement, the slight variation in conductivity may come from the increased actual surface area of the 500 nm particle-based Sn–Li, in contrast to the glassy  $2\,\mu\mathrm{m}$ -thick Sn–Li surface.

To further understand the electrochemical features of Sn-Li anodes, symmetric cells composed of a pristine Li electrode and a Sn-Li working electrode were evaluated using cyclic voltammetry (Fig. 2e). The broad peak near 100 mV corresponding to tin lithiation/delithiation is observed over multiple cycles in addition to the typical Li/Li<sup>+</sup> polarization curves, which confirms that the Sn layer on Li is electrochemically active. X-ray photoelectron spectroscopy (XPS) analysis of the cycled Sn-Li anode (Supplementary Fig. 6) reveals a SEI composed of typical materials including lithium carbonate, lithium carboxylates and fluorinated species. High-resolution scanning in the Sn 3d region shows completely attenuated peaks. These peaks become more pronounced and only slightly attenuated after multiple cycles, which testifies to the stable lithium-tin alloying without obvious SEI build-up, a result in agreement with a previous study<sup>47</sup>. The right panel in Fig. 2e compares the cyclic voltammogram of Li/Li cell and Li/Sn-Li cells. The drastic slope difference is the most significant feature. Fitting the small overpotential region of the current–overpotential  $(I-\eta)$  curve to the Tafel equation, the exchange current density can be obtained (see Supplementary Fig. 7). The exchange current (7.5 mA cm<sup>-2</sup>) for the Sn-Li anode is substantially higher than the corresponding value for Li/Li<sup>+</sup> on pristine lithium<sup>48</sup>. The fast charge transfer kinetics obtained from the exchange current density reinforces our conclusions from the impedance results that the Sn-rich SEI on lithium facilitates fast charge transfer.

Supplementary Fig. 8 compares the impedance spectra of symmetric cells using Sn-stainless steel (Sn-SS) electrodes with those

ARTICLES NATURE ENERGY

for Sn–Li. The low interfacial impedance observed relative to pristine lithium (Fig. 2c) confirms the effectiveness of the Sn coating. The electrochemical activity of the Sn coating can be examined in a straightforward manner by cyclic voltammetry, as shown in Supplementary Fig. 9. Pronounced peaks in the range of 0.3–0.8 V are associated with Li alloying reactions in Sn<sup>49</sup>. A similar electrochemical response is observed in the galvanostatic cycling measurements reported in Supplementary Fig. 10. The discharge plateau in the range 0.3–0.4 V with moderate capacity can be attributed to partial lithiation of Sn. Post-mortem SEM images of the electrodes reveal structural change after the cycling. Supplementary Fig. 11 compares SEM for Sn–SS electrodes before and after cycling. It is apparent that the Sn particle morphology is largely preserved (Supplementary Fig. 12).

## Electrochemical stability of Sn-Li hybrid anodes

A suitable artificial SEI on lithium is desirable for suppressing dendrite proliferation. Lithium electrodeposition at a 500 nm Sn—Li electrode was visualized using a custom-built optical cell (see Supplementary Fig. 13). For these experiments, Sn coatings were applied on two cylinder-shaped lithium surfaces, which are connected to the battery tester by stainless-steel transmission wires. Real-time images of the electrolyte/Sn interface can be captured at all stages of electrodeposition using an optical microscope. Figure 3a

(top) shows the evolution of the interface during electrodeposition at a current density of 4 mA cm<sup>-2</sup>. It is seen that the electrode has a smooth morphology and is essentially dendrite-free, with a visually slower growth rate compared with pristine Li. Semi-quantitative analysis can be performed on images using ImageJ software to obtain deposition thickness and roughness as a function of capacity (see Fig. 3b). Drastic morphology and roughness differences are apparent during the initial deposition of 0.5–1.0 mAh cm<sup>-2</sup>, a capacity roughly equivalent to that of the Sn coating. Electrodeposition of more lithium on the Sn-Li electrode is seen to produce a slightly rougher surface morphology, which is within expectations considering the current applied is above the diffusion limit. The overall roughness of the Sn-Li electrodes is nonetheless remarkably reduced relative to the rapid and uncontrollable mossy deposits observed for a pristine Li electrode. These results further imply that the electrochemically active Sn overlayer on the Li electrode is able to stabilize electrodeposition of Li by alloying with Li and facilitating fast interfacial transport. Similar results have been obtained in the ex situ SEM study on Sn-Li electrodes (Supplementary Fig. 14). The smooth deposit morphology remains after multiple cycles (Supplementary Fig. 15), which along with the XPS results confirms the stability of the Sn coating during Li plating/stripping.

A requirement for interface stability is that artificial interphases must be able to survive extensive cycling. Figure 3c reports that the

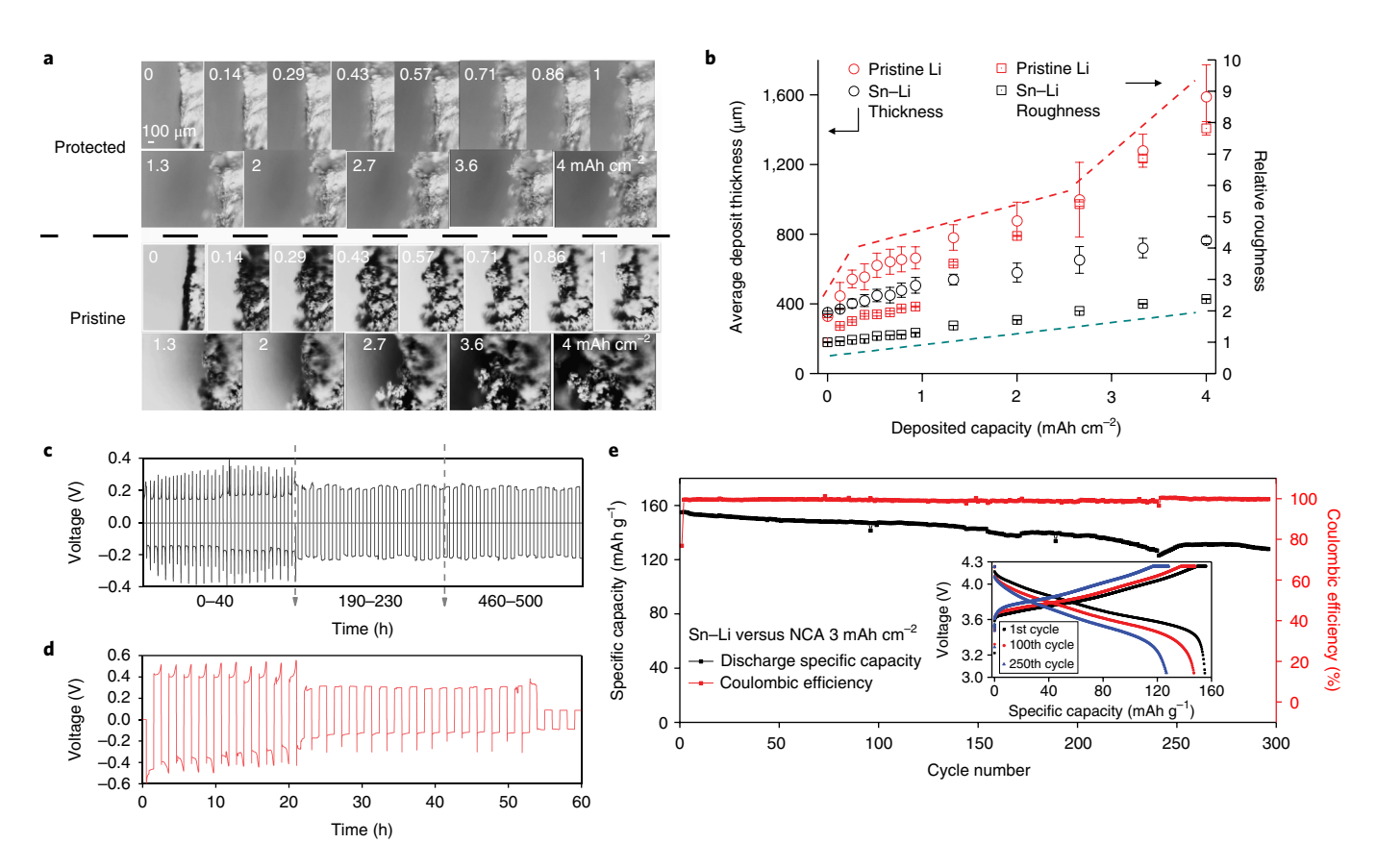


**Fig. 3 | Direct and indirect demonstrations of stability of Sn-Li hybrid anodes. a**, Capacity-sequenced optical microscopy images of the electrolyte-electrode interface during electrodeposition on Sn-Li and pristine lithium electrodes at a current density of 4 mA cm<sup>-2</sup>. The capacity (mAh cm<sup>-2</sup>) of lithium being electrodeposited on the substrate is shown in the top left corner of each image. **b**, Quantitative analysis of average deposition thickness (red) and relative roughness (black) during the deposition observed in **a**, with error bars obtained from multiple calculations of deposit area in images. The blue and red dashed lines provide rough illustrations of the increasing thickness of Sn-Li and pristine Li electrodes, respectively. The blue line displays a constant increasing rate whereas the red line reveals an accelarated thickness increase at later stages. **c**, Voltage profile of galvanostatic lithium plating/stripping on the symmetric tin-protected lithium cell at a current density of 3 mA cm<sup>-2</sup> for 1h at each step. **d**, The same experiment in **c** applied on the symmetric pristine lithium cell. **e**, Cycling profile of the tin-protected lithium versus NCA with 3 mAh cm<sup>-2</sup> areal capacity operated from 3 to 4.2 V at 0.5 C. The inset shows the voltage profile of the 1st, 100th and 200th cycle.

NATURE ENERGY ARTICLES

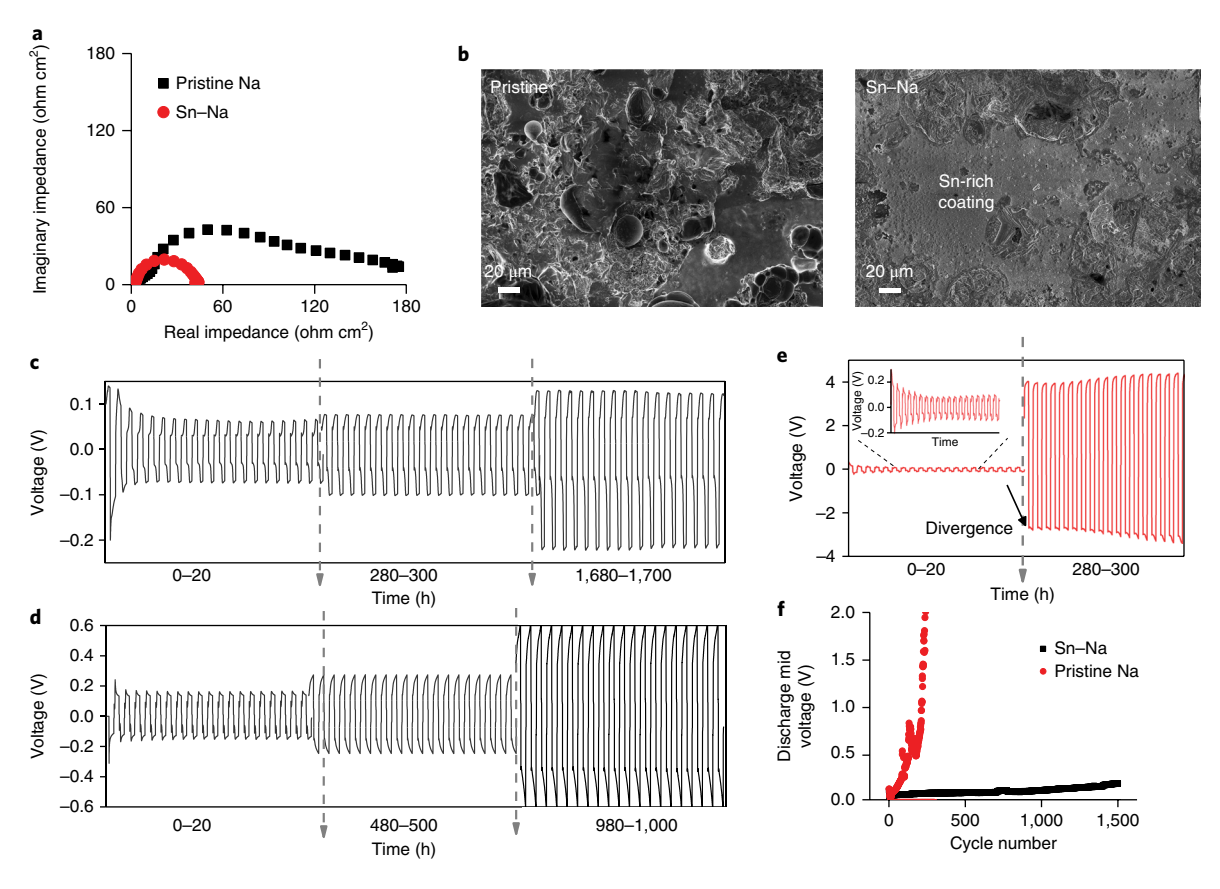


**Fig. 4 | Hybrid Sn-Na anodes offer a route to stable deposition at reactive sodium electrodes. a**, Impedance spectra of the tin-protected sodium symmetric cell and pristine sodium symmetric cell measured at room temperature. **b**, Post-mortem SEM images of the pristine sodium electrode (left) and tin-protected sodium electrode (right) after being cycled at 0.5 mA cm<sup>-2</sup> and 0.25 mAh cm<sup>-2</sup> for 10 cycles. **c**, Voltage profile of sodium plating/stripping on the symmetric tin-protected sodium cell at a current density of 0.25 mA cm<sup>-2</sup> for 1h at each step. **d**, Voltage profile of sodium plating/stripping on the symmetric tin-protected sodium cell at a current density of 0.5 mA cm<sup>-2</sup> for 0.5 h at each step. **e**, Voltage profile of sodium plating/stripping on the symmetric pristine sodium cell at a current density of 0.25 mA cm<sup>-2</sup> for 1h at each step, with the inset showing the first 20-h plot. **f**, Average discharge voltage at different cycles for the tin-protected sodium and the pristine sodium from **c**,**e**.

Sn-Li anode can be operated stably in a symmetric cell configuration at a practical current density of 3 mA cm<sup>-2</sup> and a capacity of 3 mAh cm<sup>-2</sup> per cycle. No short-circuit is observed during a 500-h period of continuous measurement, as opposed to the control, which exhibits permanent failure, evidenced by the sudden voltage drop after approximately 55 h (see Fig. 3d and Supplementary Fig. 16). The stability of the Sn-Li anode makes it a promising candidate for new types of Li battery that rely on a combination of plating and alloying processes for achieving stable, long-term operation. Figure 3e shows that such cells can be operated in prototype full cell configurations paired with state-of-the-art intercalating cathodes (NCA) with high loading (19.9 mg cm<sup>-2</sup>; 3 mAh cm<sup>-2</sup>); the inset reports the voltage-capacity profile. A capacity retention of >80% is observed over 300 cycles of operation at a rate of 0.5 C with Coulombic efficiency close to unity (Supplementary Fig. 17). Similar stable operation has also been observed in cells equipped with LiCoO2 cathodes (Supplementary Fig. 18), which testifies to the broad compatibility of the Sn-Li hybrid anodes studied here. A stable Li-electrolyte interface means that cells based on thinner Li anodes should be possible. To explore this possibility, we studied Sn-Li/NCA cells in which the anode/cathode capacity ratio is fixed at 3:1 (Supplementary Fig. 19). In contrast to cells that use pristine lithium, which fail quickly within 30 cycles, the Sn-Li/ NCA cells cycle stably for over 100 cycles. Post-mortem analysis (Supplementary Fig. 20) reveals that thickened SEI forms as a result of electrolyte decomposition; despite this, the surface morphology

is observed to remain flat. This, in principle, will increase the interface impedance, underscoring the need for additional efforts to optimize the electrolyte composition for Sn–Li anodes for further improvements in cell performance.

# Stabilizing sodium metal electrodes with metallic tin

The success of the Sn-Li hybrid electrodes leads one to wonder whether the same concept might be applied to achieve stability of sodium anodes, notorious for their reactivity with carbonate electrolytes and propensity to form rough, dendritic deposits during battery recharge. To evaluate this, Sn-Na hybrid electrodes were prepared in a similar manner based on ion exchange with a Sn salt additive in a liquid carbonate electrolyte. Figure 4a compares the impedance spectra measured at room temperature for the pristine symmetric sodium cell and symmetric Sn-Na cells, both in a 1 M NaPF<sub>6</sub>-EC/propylene carbonate-based electrolyte. The interfacial resistance of the Sn-Na cells is evidently significantly reduced compared with the pristine case. In contrast to lithium, the Sn layer on sodium is mostly in the form of a sodium-rich alloy instead of the metal, as evidenced by the XRD profile (Supplementary Fig. 21). Some oxide peaks are observed as a result of swift reaction of sodium in the environment. This can be attributed to the high reactivity of the sodium electrode and its fast transport in Sn. After cycling symmetric cells, both pristine and Sn-Na electrodes were harvested and observed using SEM (Fig. 4b). The pristine sodium forms irregular bumps covering the surface, probably due ARTICLES NATURE ENERGY

to the non-uniform, fragile SEI formation because of the electrolyte decomposition. On the other hand, the surface of the Sn-Na electrode maintains a flat, uniform morphology. A protected electrode surface is particularly critical for long-term battery operation. As a proof-of-concept, the symmetric sodium cells were subjected to repeated charge/discharge cycles at moderate current densities of 0.25 and 0.5 mA cm<sup>-2</sup>, as shown in Fig. 4c,d. Sodium metal batteries typically fail quickly due to the resistive SEI formed by uncontrolled side reactions between sodium and essentially all liquid electrolytes, which manifests in a tell-tale voltage divergence at the end of life. In contrast to this expectation, the Sn-Na symmetric cells exhibit drastically improved voltage profiles over extensive cycling, with only a slight increase in the overpotential. As expected, the pristine sodium cell exhibits a quick voltage divergence to 1V after merely 250h even at the low current density (Fig. 4e,f). We further demonstrate a proof-of-concept investigation on a Sn-Na/sodium manganese hexacyanoferrate battery. The results reported in Supplementary Fig. 22 show that the typical voltage profiles<sup>50</sup> are observed for this cell chemistry and that the profiles are stable over multiple cycles of charge and discharge. These results support the feasibility of the Sn-Na hybrid anode for Na-based batteries. Our results also imply that Sn protection of reactive metal anodes provides a versatile route towards hybrid anodes that take advantage of alloying and plating processes for stable, high-energy electrochemical storage.

## Conclusion

We report that hybrid anodes created by depositing Sn on the surface of reactive alkali metals such as Li and Na via a facile ion-exchange reaction provide a mechanism for protecting the anode and at the same time facilitate fast charge transfer kinetics at the electrode. We find that Sn-Li and Sn-Na anodes exhibit vastly reduced interfacial impedance and much higher exchange current in liquid electrolytes. These observations are attributed to utilization of a combination of metal electrodeposition and alloying for hybrid charge storage and fast interfacial charge transport. Sn-Li anodes are also reported by means of direct visualization studies in an optical microscope and ex situ electron microscopy measurements to exhibit stable long-term galvanostatic cycling without forming dendrites. The excellent stability of Sn-Li is further demonstrated in studies utilizing the material as the anode for lithium metal batteries where it is paired with a high-loading (19.9 mg cm<sup>-2</sup>, 3 mAh cm<sup>-2</sup>) NCA cathode. Motivated by these observations, we create and study hybrid Sn-Na anodes and report that they enable exceptionally stable electrodeposition of the notoriously unstable metal sodium. Over 1,600 h of steady operation of symmetric Sn-Na cells can be achieved at moderate current densities, with no signs of voltage divergence typically observed in Na cells based on aprotic liquid electrolytes.

# Methods

Fabrication of the protected lithium metal anode. Lithium metal foil was purchased from MTI and stored in a sub-ppm argon-filled glovebox (Inert Inc.) before use without additional treatment. Tin bis(trifluoromethanesulfonyl) imide (SnTFSI, Alfa Aesar) was dissolved in ethylene carbonate/dimethyl carbonate (EC/DMC, 1:1 v/v) with different concentrations and the resultant clear solution was used to pretreat lithium metal foil to form surface protection. One hundred microlitres of SnTFSI solution was dropped on the lithium surface and the reaction was allowed to proceed for 30 min. Treated lithium metal appears dark grey on the surface and was dried in the glovebox antechamber before use. The Sn coating can also be transferred to an inert stainless steel by gently pressing the treated lithium metal on the stainless steel. As-obtained Sn-stainless steel electrodes could be directly used for characterization. Sodium cubes (Sigma-Aldrich) were stored in mineral oil and sliced with fresh inner exposed for the same surface treatment.

Materials characterization. A Leo 1550 Keck field-emission scanning electron microscope with a Bruker EDX detector and an FEI Strata 400 DualBeam focused ion beam (FIB) fitted with a Quorum PP3010T Cryo-FIB/SEM Preparation System were used to characterize the surface morphology and cross-section morphology of the tin-protected alkali metal. To avoid reaction of the lithium sample with  $\rm O_2$  and moisture in the ambient air during cryo-FIB experiments, the

samples were quickly plunged into a nitrogen slush immediately after treatment or harvesting from lithium cells. To confirm the chemical stability of lithium in liquid nitrogen, a scan of the EDX spectrum of a pristine lithium frozen undergoing the same treatment was conducted, which showed no detectable nitrogen signal (Supplementary Fig. 1). The samples were subsequently maintained at −165 °C in the cryo-FIB to preserve their structure. After cooling, all samples investigated remained under liquid nitrogen or in vacuum for the duration of the experiment. The crystal structure of the tin-protected lithium/sodium was investigated using a Rigaku X-Ray diffractometer from 20 to 80 degrees (two theta). Tin-protected sodium metal was wrapped in Kapton tape during the experiment to avoid oxidation in air. Tin-protected lithium metal was measured directly to gain the best resolution, since the surface treatment significantly slows down the oxidation. X-ray photoelectron spectroscopy SSX-100 (XPS) was used to study the detailed chemistry information on the tin-protected lithium surface. To avoid surface contamination, a vacuum puck was used to transfer samples from the argon-filled glovebox to the high-vacuum XPS chamber without exposure to the atmosphere.

**Electrochemical characterization.** Electrochemical studies were performed using CR2032 coin cells with symmetric and asymmetric designs. Symmetric lithium cells were assembled with two tin-treated lithium metal anodes (Sn-Li/Sn-Li), a Celgard 3501 polypropylene separator, and electrolyte containing 1 M LiPF6 in EC/DMC (1:1) with 10 v% fluorinated ethylene carbonate and 1 vol% vinylene carbonate. For cyclic voltammetry measurement, symmetric lithium cells with pristine lithium and tin-treated lithium (Li/Sn-Li) were used. Symmetric sodium cells were assembled with two tin-treated sodium metal anodes (Sn-Na/Sn-Na). a Celgard 3501 polypropylene separator, and electrolyte containing 1 M NaPF<sub>6</sub> in EC/propylene carbonate (1:1 vol%). Asymmetric lithium cells composed of a tin-treated lithium metal anode with a thickness of 450 um and lithium nickel cobalt aluminium oxide (NCA) cathodes (Sn-Li/NCA) were provided by the CAMP facility at Argonne National Labs; these had a 90% active material loading and an area capacity of 3 mAh cm<sup>-2</sup>. A piece of glass fibre was added in the prototype full cell to absorb sufficient electrolyte (200  $\mu$ l, about 110  $\mu$ l remained in the cell after the cell crimping). For 3:1 anode to cathode capacity ratio Sn-Li/NCA cells, lithium was first deposited on stainless steel with the predetermined capacity (9 mAh cm<sup>-2</sup>, which corresponds to a thickness of about 45 μm) in 1 M LiTFSI DOL/DME (1:1), whose surface was thoroughly cleaned with DOL solvent and dried. Then the same Sn ion exchange process was applied to achieve the Sn-Li anode, as described previously.

Temperature-dependent ionic conductivity and impedance spectra were measured from  $10^7\,Hz$  to  $10^{-1}\,Hz$  at a temperature range of -5 to  $100\,^{\circ}C$  using a Novocontrol dielectric/impedance spectrometer coupled with a temperature-controlling chamber. Cyclic voltammetry was performed on a CH 600E potentiostat with lithium being the pseudo-reference electrode at a sweep rate of  $1\,mV\,s^{-1}$ . Galvanostatic plating/stripping of symmetric cells was studied on Neware battery testers at room temperature. Sn–Li/NCA prototype full cells were cycled using a constant current–constant voltage charge and constant current discharge from 3 to 4.2 V.

The in situ observation cell (illustrated in Supplementary Fig. 13) was homemade and fitted in the stage of an upright optical microscope (Nikon Optiphot) equipped with an objective with an extra-long working distance. Two lithium cylinder rods with a diameter of half an inch were used as the electrodes connected with stainless-steel transmission lines to the battery test channels. The snapshots were taken using an Olympus camera and a microscope with ×100 magnification. Images analysis was performed using ImageJ software. Parameters are defined as the ratio between the two-dimensional image area from the measurement and the theoretical value assuming a dense, flat deposit.

**Data availability.** The data that support the plots within this paper and other findings of this study are available from the corresponding author upon reasonable request.

Received: 1 August 2017; Accepted: 22 January 2018; Published online: 05 March 2018

#### References

- Armand, M. & Tarascon, J. M. Building better batteries. Nature 451, 652–657 (2008)
- Goodenough, J. B. & Kim, Y. Challenges for rechargeable Li batteries. Chem. Mater. 22, 587–603 (2009).
- Bruce, P. G. Energy storage beyond the horizon: Rechargeable lithium batteries. Solid State Ion. 179, 752–760 (2008).
- Whittingham, M. S. Electrical energy storage and intercalation chemistry. Science 192, 1126–1127 (1976).
- Xu, W. et al. Lithium metal anodes for rechargeable batteries. Energy Environ. Sci. 7, 513–537 (2014).
- Tikekar, M. D., Choudhury, S., Tu, Z. & Archer, L. A. Design principles for electrolytes and interfaces for stable lithium-metal batteries. *Nat. Energy* 1, 16114 (2016).

NATURE ENERGY ARTICLES

- Lin, D., Liu, Y. & Cui, Y. Reviving the lithium metal anode for high-energy batteries. Nat. Nanotech. 12, 194–206 (2017).
- Tarascon, J. M. & Armand, M. Issues and challenges facing rechargeable lithium batteries. *Nature* 414, 359–367 (2001).
- Aurbach, D., McCloskey, B. D., Nazar, L. F. & Bruce, P. G. Advances in understanding mechanisms underpinning lithium-air batteries. *Nat. Energy* 1, 16128 (2016).
- Ma, L., Hendrickson, K. E., Wei, S. & Archer, L. A. Nanomaterials: science and applications in the lithium-sulfur battery. *Nano Today* 10, 315–338 (2015).
- Li, Y. & Dai, H. Recent advances in zinc-air batteries. Chem. Soc. Rev. 43, 5257–5275 (2014).
- 12. Wei, S. et al. A stable room-temperature sodium-sulfur battery. *Nat. Commun.* 7, 11722 (2016).
- Al Sadat, W. I. & Archer, L. A. The O<sub>2</sub>-assisted Al/CO 2 electrochemical cell: A system for CO<sub>2</sub> capture/conversion and electric power generation. *Sci. Adv.* 2, e1600968 (2016).
- Tu, Z., Nath, P., Lu, Y., Tikekar, M. D. & Archer, L. A. Nanostructured electrolytes for stable lithium electrodeposition in secondary batteries. *Acc. Chem. Res.* 48, 2947–2956 (2015).
- Cheng, X. B. et al. A review of solid electrolyte interphases on lithium metal anode. Adv. Sci. 3, 1500213 (2016).
- Xu, K. Electrolytes and interphases in Li-ion batteries and beyond. Chem. Rev. 114, 11503–11618 (2014).
- 17. Verma, P., Maire, P. & Novák, P. A review of the features and analyses of the solid electrolyte interphase in Li-ion batteries. *Electrochim. Acta* 55, 6332–6341 (2010).
- Ji, L., Lin, Z., Alcoutlabi, M. & Zhang, X. Recent developments in nanostructured anode materials for rechargeable lithium-ion batteries. *Energy Environ. Sci.* 4, 2682–2699 (2011).
- Khurana, R., Schaefer, J. L., Archer, L. A. & Coates, G. W. Suppression of lithium dendrite growth using cross-linked polyethylene/poly(ethylene oxide) electrolytes: a new approach for practical lithium-metal polymer batteries. J. Am. Chem. Soc. 136, 7395–7402 (2014).
- Tung, S.-O., Ho, S., Yang, M., Zhang, R. & Kotov, N. A. A dendritesuppressing composite ion conductor from aramid nanofibres. *Nat. Commun.* 6, 6152 (2015)
- Fergus, J. W. Ceramic and polymeric solid electrolytes for lithium-ion batteries. J. Power Sources 195, 4554–4569 (2010).
- Lu, Y., Korf, K., Kambe, Y., Tu, Z. & Archer, L. A. Ionic-liquid-nanoparticle hybrid electrolytes: applications in lithium metal batteries. *Angew. Chem. Int.* Ed. 53, 488–492 (2014).
- 23. Villaluenga, I. et al. Compliant glass–polymer hybrid single ion-conducting electrolytes for lithium batteries. *Proc. Natl Acad. Sci. USA* **113**, 52–57 (2016).
- Tu, Z., Lu, Y. & Archer, L. A Dendrite-free lithium metal battery model based on nanoporous polymer/ceramic composite electrolytes and high-energy electrodes. Small 11, 2631–2635 (2015).
- Tu, Z. et al. Nanoporous hybrid electrolytes for high-energy batteries based on reactive metal anodes. Adv. Energy Mater. 7 7, 1602367 (2017).
- Monroe, C. & Newman, J. The impact of elastic deformation on deposition kinetics at lithium/polymer interfaces. *J. Electrochem. Soc.* 152, A396–A404 (2005).
- Bouchet, R. et al. Single-ion BAB triblock copolymers as highly efficient electrolytes for lithium-metal batteries. Nat. Mater. 12, 452–457 (2013).
- Ma, Q. et al. Single lithium-ion conducting polymer electrolytes based on a super-delocalized polyanion. Angew. Chem. Int. Ed. 55, 2521–2525 (2016).
- Lu, Y. et al. Stable cycling of lithium metal batteries using high transference number electrolytes. Adv. Energy Mater. 5, 1402073 (2015).
- 30. Wei, S. et al. Highly stable sodium batteries enabled by functional ionic polymer membranes. *Adv. Mater.* **29**, 1605512 (2017).
- Lee, Y. M. et al. Effects of triacetoxyvinylsilane as SEI layer additive on electrochemical performance of lithium metal secondary battery. *Electrochem. Solid-State Lett.* 10, A216–A219 (2007).
- Zhang, X. Q., Cheng, X. B., Chen, X., Yan, C. & Zhang, Q. Fluoroethylene carbonate additives to render uniform Li deposits in lithium metal batteries. Adv. Funct. Mater. 27, 1605989 (2017).
- 33. Zheng, G. et al. High-performance lithium metal negative electrode with a soft and flowable polymer coating. ACS Energy Lett. 1, 1247–1255 (2016).
- Ma, L., Kim, M. S. & Archer, L. A. Stable artificial solid electrolyte interphases for lithium batteries. *Chem. Mater.* 29, 4181–4189 (2017).
- Liu, Y. et al. An artificial solid electrolyte interphase with high Li-ion conductivity, mechanical strength, and flexibility for stable lithium metal anodes. Adv. Mater. 29, 1605531 (2017).

- Li, J., Dudney, N. J., Nanda, J. & Liang, C. Artificial solid electrolyte interphase to address the electrochemical degradation of silicon electrodes. ACS Appl. Mater. Interfaces 6, 10083–10088 (2014).
- Choudhury, S., Agrawal, A., Wei, S., Jeng, E. & Archer, L. A. Hybrid hairy nanoparticle electrolytes stabilizing lithium metal batteries. *Chem. Mater.* 28, 2147–2157 (2016).
- Kim, M. S., Ma, L., Choudhury, S. & Archer, L. A. Multifunctional separator coatings for high-performance lithium. Adv. Mater. Interfaces 3, 1600450 (2016).
- Han, X. et al. Negating interfacial impedance in garnet-based solid-state Li metal batteries. *Nat. Mater.* 16, 572–579 (2017).
- Lin, D. et al. Layered reduced graphene oxide with nanoscale interlayer gaps as a stable host for lithium metal anodes. *Nat. Nanotech.* 11, 626–632 (2016).
- Liang, Z. et al. Composite lithium metal anode by melt infusion of lithium into a 3D conducting scaffold with lithiophilic coating. *Proc. Natl Acad. Sci.* USA 113, 2862–2867 (2016).
- 42. Tu, Z., Choudhury, S., Wei, S. & Archer, L. Surface Protected Active Metal Electrodes for Rechargeable Batteries. PCT/US2017/067358 (2017).
- Lou, X. W., Wang, Y., Yuan, C., Lee, J. Y. & Archer, L. A. Template-free synthesis of SnO<sub>2</sub> hollow nanostructures with high lithium storage capacity. Adv. Mater. 18, 2325–2329 (2006).
- Winter, M. & Besenhard, J. O. Electrochemical lithiation of tin and tin-based intermetallics and composites. *Electrochim. Acta* 45, 31–50 (1999).
- Choi, Y.-S., Byeon, Y.-W., Ahn, J.-P. & Lee, J.-C. Formation of Zintl ions and their configurational change during sodiation in Na–Sn battery. *Nano Lett.* 17, 679–686 (2017).
- Nesper, R. Structure and chemical bonding in Zintl-phases containing lithium. Prog. Solid State Chem. 20, 1–45 (1990).
- Li, J.-T. et al. XPS and ToF-SIMS study of Sn-Co alloy thin films as anode for lithium ion battery. J. Power Sources 195, 8251-8257 (2010).
- Munichandraiah, N., Scanlon, L. & Marsh, R. Surface films of lithium: an overview of electrochemical studies. J. Power Sources 72, 203–210 (1998).
- Zhang, W. M. et al. Tin-nanoparticles encapsulated in elastic hollow carbon spheres for high-performance anode material in lithium-Ion batteries. *Adv. Mater.* 20, 1160–1165 (2008).
- Wang, L. et al. A superior low-cost cathode for a Na-ion battery. Angew. Chem. Int. Ed. 52, 1964–1967 (2013).

# Acknowledgements

This work was supported by the Department of Energy (DOE), Advanced Research Projects Agency - Energy (ARPA-E) through award no. DE-AR0000750. M.J.Z. and L.F.K. acknowledge support by the NSF (DMR-1654596). The work made use of electrochemical characterization facilities in the KAUST-CU Centre for Energy and Sustainability, supported by the King Abdullah University of Science and Technology (KAUST) through award no. KUS-C1-018-02. Electron microscopy facilities at the Cornell Centre for Materials Research (CCMR), an NSF-supported MRSEC through Grant DMR-1120296, were also used for the study. Additional support for the FIB/SEM cryo-stage and transfer system was provided by the Kavli Institute at Cornell and the Energy Materials Centre at Cornell, DOE EFRC BES (DE-SC0001086). Z.T. thanks B. Polzin for kindly providing NCA cathode materials from the Cell Analysis, Modeling, and Prototyping (CAMP) Facility at Argonne National Laboratories.

# **Author contributions**

Z.T. and L.A.A. conceptualized the project. Z.T., S.C., M.J.Z., L.F.K. and L.A.A. developed the methodology. Z.T., S.C., M.J.Z. and S.W. conducted all experiments reported in the paper. Z.T. and L.A.A. wrote the original draft. Z.T., S.C., M.J.Z., L.F.K. and L.A.A. further wrote and revised the manuscript. L.F.K. and L.A.A. acquired funding for the work and supervised the research reported in the paper.

## Competing interests

The authors declare no competing interests.

# Additional information

**Supplementary information** is available for this paper at https://doi.org/10.1038/s41560-018-0096-1.

Reprints and permissions information is available at www.nature.com/reprints.

Correspondence and requests for materials should be addressed to L.A.A.

**Publisher's note:** Springer Nature remains neutral with regard to jurisdictional claims in published maps and institutional affiliations.